A Highly Sensitive and Selective Turn-On Fluorogenic and Chromogenic Sensor Based on BODIPY-Functionalized Magnetic Nanoparticles for Detecting Lead in Living Cells

Hyunjong Son,[a] Hye Young Lee,[a] Jung Mi Lim,[b] Dongmin Kang,*[b] Won Seok Han,[a] Shim Sung Lee,[a] and Jong Hwa Jung*[a]

Metal ions can pose severe risks for human health and the environment, and thus methods for the facile preparation of fluorogenic and chromogenic receptors with high selectivity and sensitivity for heavy metal ions have continued to receive much interest.[1] Among heavy metal ions, Pb^{2+} is one of the most dangerous, causing adverse health effects from lead exposure, particularly in children.[2] A variety of symptoms have been attributed to lead poisoning. Once introduced into the body, Pb^{2+} can cause abdominal pain and vomiting. The long accumulation of Pb^{2+} in the body leads to many serious human health problems, including muscle paralysis, mental confusion, memory loss, and anaemia; this suggests that Pb^{2+} affects multiple targets in vivo.[3] Plausible molecular targets of lead include calcium- and zinc-binding proteins that control cell signaling and gene expression, respectively.[4] Thus, it is important to develop a safe and effective procedure to detect and remove lead from the body following toxic lead contamination.[5]

Magnetic silica nanoparticles are of great interest for biomedical and environmental research applications such as bioseparation, drug targeting, cell isolation, enzyme immobilization, and protein purification, because of their biocompatibility and stability against degradation.[6] In particular, magnetic silica nanoparticles can be easily modified with a wide range of functional groups. For example, incorporation of chromophores in silica nanoparticles provides magnetic and luminescent core/shell nanoparticles with applications as contrast agents for molecular imaging.[7]

It is clear that the receptor-immobilized magnetic nanoparticles have some important advantages as a solid chemosensor and adsorbent in heterogeneous solid–liquid phases.[8] First, such nanoparticles are readily synthesized by sol–gel condensation, a versatile technique that allows chemical functionalities. Second, immobilized receptors on an inorganic support can remove the guest molecules (toxic metal ions and anions) from the pollutant solution. Third, the magnetic nanoparticles can be easily isolated from pollutants by a small magnet and repeatedly utilized with suitable treatment. In particular, the magnetic nanoparticles can also provide efficient binding to the guest molecules because their high surface-to-volume ratio simply offers more contact area.

In the above context, the design of fluorescent probes for the detection of lead ion is of especial interest due to the selective, sensitive, nondestructive, and rapid nature of fluorescence emission signals.[9] However, most of the probes described thus far do not have high selectivity for Pb^{2+} over other metal ions and, in general, they cannot be used for aqueous systems.[10] Thus, Chen and co-wokers described a Pb^{2+} ion sensor where the fluorescence intensity enhancement was about 18-fold in the presence of Cu^{2+} (100 equiv) in acetonitrile.[5d] Yoon and co-workers reported a selective sensor for Pb^{2+} ion employing a rhodamine B-based fluorescent receptor for use in acetonitrile.[10a] We have also reported a Pb^{2+} sensor based on a 4,4-difluoro-4-bora-3a,4a-diaza-s-indacene (hereafter abbreviated to BODIPY) receptor with a fluorescence intensity enhancement of only about 25-fold.[5d]

Very recently, the use of nanoparticles as solid supports in combination with supramolecular concepts has led to the development of new hybrid nanomaterials with improved functionalities that offer much promise for use in the development of simple and efficient sensors of heavy metal ions in

[a] H. Son, H. Y. Lee, Dr. W. S. Han, Prof. Dr. S. S. Lee,
Prof. Dr. J. H. Jung
Department of Chemistry and Research Institute of Natural Sciences
Gyeongsang National University, Jinju 660-701 (Korea)
Fax: (+82)55-758-6027
E-mail: jonghwa@gnu.ac.kr

[b] J. M. Lim, Prof. Dr. D. Kang
Division of Life and Pharmaceutical Sciences
EwhaWomans University, Seoul 120-750 (Korea)

Supporting information for this article is available on the WWW under http://dx.doi.org/10.1002/chem.201001772.

biological, toxicological, and environmental applications.[8b,11–13] Although a number of signalling systems for the detection of heavy metal ions are now known,[8b,11,14–16] there are no precedents for the use of hybrid nanoparticles to detect Pb^{2+} that employ a dual signal fluoro-chromophore that operates via a "turn-on" approach. We now describe the construction of the new off–on fluorescent Pb^{2+} sensor **1** that operates via a PET (photoinduced electron transfer) mechanism. Sensor **1** was shown to be highly sensitive and selective for Pb^{2+} in pure aqueous solution. The application of the new sensor for the detection of lead ion in living cells is also described (see Scheme 1). To minimize the background fluorescence of the free sensor, a diethylamino group as an electron-donating group was introduced and a styryl group was attached to a BODIPY fluorophore to induce enhancement of the absorption intensity as well as to induce a large red shift in UV/Vis absorption band of interest.
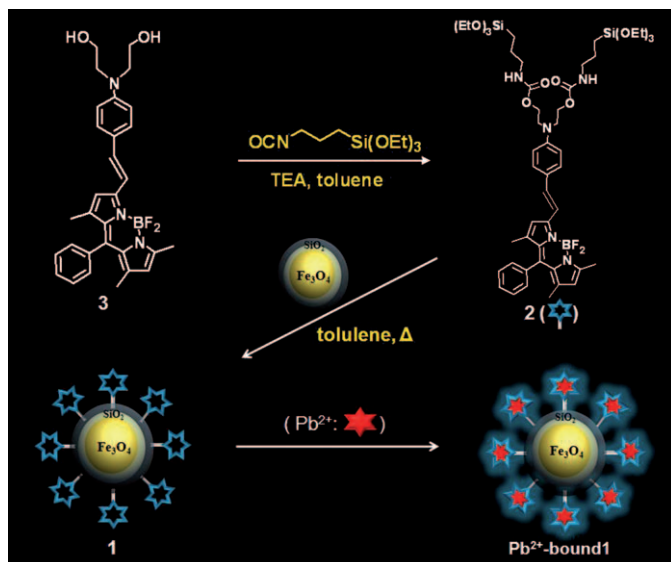
Scheme 1. Preparation of BODIPY-functionalized $Fe_3O_4@SiO_2$ core/shell nanoparticle (**1**).

In order to obtain a highly sensitive and selective off–on sensor for Pb^{2+} in aqueous solution for practical application, a BODIPY moiety was employed as the fluorophore/chromophore because of its characteristic strong absorption and fluorescence behavior (including high fluorescence quantum yields) and its high chemical stability. $Fe_3O_4@SiO_2$ core/shell nanoparticles were employed as the inorganic support because of their light yellow color and the ease of their magnetic separation.

The encapsulation of Fe_3O_4 nanocrystals within silica shells was conducted in a microemulsion system in water droplets using 4 nm-sized Fe_3O_4 nanocrystals in an external cyclohexane phase. The formation of the silica shell around the Fe_3O_4 nanocrystals was carried out by the addition of an NH_4OH aqueous solution followed by tetraethyl orthosili-

cate (TEOS) and the reaction was allowed to proceed or 24 h (Scheme S1).

Compound **3** was synthesized following a similar method to that described previously (Scheme S2).[11a] The $Fe_3O_4@SiO_2$ core/shell nanoparticles were reacted with **2** in toluene with vigorous stirring overnight to covalently link them onto the surface of the $Fe_3O_4@SiO_2$ nanoparticles by a sol–gel reaction (see Experimental Section and Scheme 1). Compound **1** was fully characterized by transmission electron microscopy (TEM), FTIR spectroscopy, time-of-flight second ion mass spectroscopy (TOF-SIMS), and fluorophotometry.

A TEM image of **1** revealed a spherical structure with a narrow size distribution (ca. 20 nm) and a 4 nm Fe_3O_4 nano core, which maintained its nanocrystalline appearance (Figure 1). The IR and TOF-SIMS results were in accord with bond formation; the IR spectrum of **1**, showed strong new bands at $\tilde{\nu} = 3379, 2919, 2850, 2359, 1640, 1568, 1465, 1441, 1389, 1293,$ and $1054\ cm^{-1}$ which originated from receptor **2** in accordance with **2** now residing on the $Fe_3O_4@SiO_2$ core/shell nanoparticles (Figure S1). The TOF-SIMS spectrum of **1** displayed fragments attributable to **2** (m/z 325, 338, 422), thereby providing evidence that **2** was anchored onto the surface of the $Fe_3O_4@SiO_2$ core/shell nanoparticles (Figure S2).
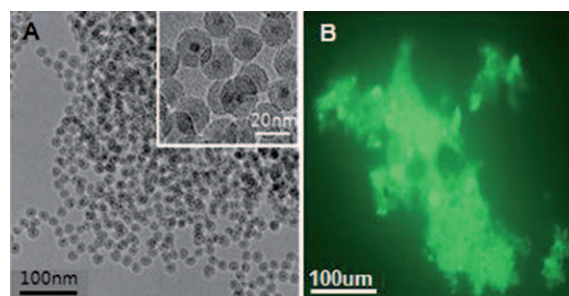

Figure 1. A) TEM image of **2**-immobilized $Fe_3O_4@SiO_2$ core/shell nanoparticles (**1**). B) Fluorescence microscope image of Pb^{2+}-bound **1**.

Spectroscopic measurements for **1** were performed in 20 mM HEPES (4-(2-hydroxyethyl)-1-piperazineethanesulfonic acid) buffer, pH 7.4. The UV/Vis absorption spectrum of free **1** showed two absorption bands at 324 and 596 nm ($\varepsilon = 3.20 \times 10^4$ and $4.50 \times 10^4\ M^{-1}cm^{-1}$, respectively). The absorption maximum at 596 nm for **1** was redshifted in its UV/Vis absorbance by almost 70 nm relative to the behavior reported previously by our group,[11a] for a BODIPY parent system without the styryl group. When Pb^{2+} was added gradually to the above spectrophotometric solution the λ_{abs} showed a 45 nm blue shift with an isosbestic point occurring at 570 nm; the color of the solution turned from light blue to pale red (Figure S3a). As expected, **1** is virtually non-fluorescent in its apo state ($\Phi < 0.0005$, $\lambda_{ex} = 326$ nm), which is a consequence of the efficient photoinduced electron transfer (PET)[17–19] quenching of the fluorophore by the lone pair electrons of the nitrogen atom in the benzoyl

moiety. Upon addition of increasing Pb^{2+} concentrations, **1** showed a large CHEF (chelation-enhanced fluorescence) effect in the fluorescence emission spectra, that results from the blocking of the PET process and an overall emission change of approximately 100-fold ($\Phi = 0.054$, Figure 2 a) at the emission maximum ($\lambda_{em} = 460$) was observed.
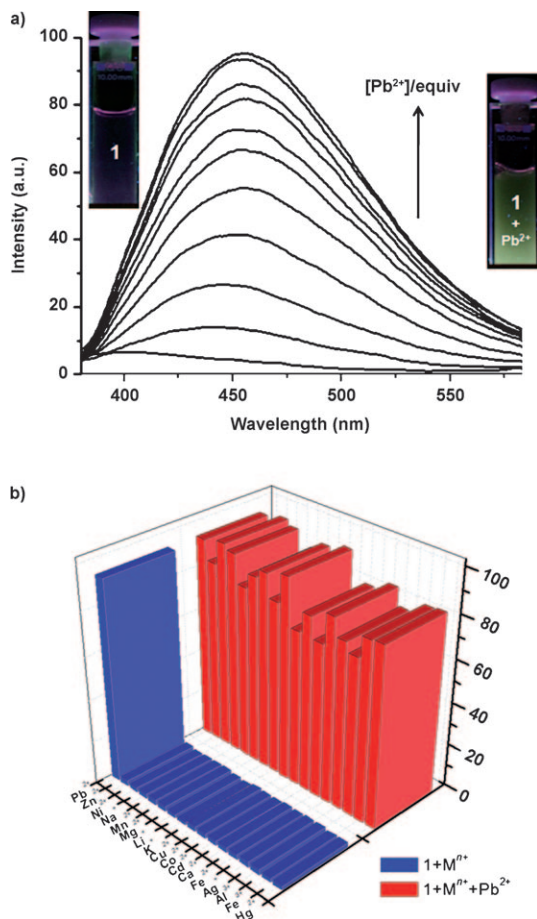

Figure 2. A) Fluorescence responses of **1** (10 μM) upon addition of increasing Pb^{2+} concentrations (0, 25, 50, 75, 100, 125, 150, 175, 200, 225, and 250 equiv) in 20 mM HEPES in pure aqueous solution at pH 7.4 ($\lambda_{ex} = 326$ nm). B) Fluorescence responses of **1** to various metal ions. Blue bars represent the addition of selected metal ions (250 equiv) to a 10 μM solution of **1**. Red bars represent subsequent addition of Pb^{2+} (250 equiv) to the solution. For all measurements, the pH value was adjusted by using 20 mM HEPES in pure aqueous solution, pH 7.4. Excitation was provided at 326 nm, and the emission was monitored at 460 nm.

With few exceptions,[20] most reported BODIPY-fluorescent sensors are based on an intramolecular charge transfer (ICT) mechanism.[17,19] However, in our case, the noticeable fluorescence intensity enhancement of the receptor **2** attached to $Fe_3O_4@SiO_2$ core/shell nanoparticles may be due to the inhibition of the PET process during the binding of Pb^{2+}. Preliminary computational simulations indicated that **2** is twisted at the BODIPY moiety, presumably resulting in a blocking of the ICT. In addition, the amine being directly conjugated to the styryl group results in a very significant

red shift, and high fluorescence quantum yields for this BODIPY-based receptor.[17a] These previous results are in complete accord with our present observations.[16a]

We also investigated the binding ability of **1** as an ion-selective fluoro-chromogenic probe for the other metal ions Ca^{2+}, Hg^{2+}, Cd^{2+}, Li^+, Ag^+, Cu^{2+}, Fe^{2+}, Mg^{2+}, Zn^{2+}, K^+, Na^+, Mn^{2+}, Co^{2+}, Fe^{3+}, Al^{3+}, and Ni^{2+}. However, no significant spectral changes were observed upon addition of any of these metal ions (Figure S 3b), indicating that **1** is a highly selective chemosensor for the detection of Pb^{2+}.

For comparison, we performed spectroscopic measurements using **2** in an acetonitrile solution (this solvent was employed due to the insolubility of **2** in water); under these conditions **2** gave two absorption bands at 324 and 596 nm ($\varepsilon = 3.25 \times 10^4$ and $5.0 \times 10^4\,M^{-1}\,cm^{-1}$, respectively). In the absence of Pb^{2+}, **2** also exhibited no fluorescence emission when excited at 326 nm. Upon the addition of Pb^{2+}, for the case of chemosensor **1**, the absorption band at 596 nm was blue shifted by 45 nm, but the fluorescence emission intensity of **2** increased by approximately 80-fold ($\Phi = 0.042$, Figure S4) with an emission maximum at 456 nm. The fluorescence intensity enhancement of **1** compared to **2** is likely due to its preorganized structure on the surface of the nanoparticles.

The highly selective Pb^{2+} recognition of fluorescence chemosensor **1** demonstrates that the approach employed in the present study is capable of cooperatively enhancing and controlling the selectivity towards this metal ion. More importantly, quantitative measurements of the emission maximum of Pb^{2+}-bound **1** indicated that the fluorescence change correlated linearly with the [Pb^{2+}] over the 0–30 ppb range investigated. We determined that the limit of detection of **1** for Pb^{2+} is 1.5 ppb, more than sufficient to sense the Pb^{2+} concentration in drinking water with respect to the US EPA limit (15 ppb). An evaluation of the time course for the fluorescence intensity of **1** at 460 nm (Figure S5) indicated that immediately after the addition of Pb^{2+}, the fluorescence intensity of **1** started to increase and that by 60 s the fluorescence intensity was almost saturated. Thus, the response time of this system is within 1 min, making it a rapid and convenient method for the quantitation of Pb^{2+} in aqueous solution (Figure S6).

The regeneration of **1** after exposure to Pb^{2+} was examined. The Pb^{2+}-bound **1** was treated with an aqueous EDTA solution (10 μM). As expected, upon the addition of the solution, the fluorescence intensity of Pb^{2+}-bound **1** was quenched. However, when the washed, stripped nanoparticles **1** were re-exposed to Pb^{2+}, the fluorescence emission was again present, with no decrease in response (Figure S7). The fluorescence change was reproducible over several cycles of detection/stripping. The Job plot using the fluorescence changes indicated 1:1 binding for **1** with Pb^{2+} (Figure S8). Using the fluorescence titration data, the association constant (K) for Pb^{2+} coordination to **1** was calculated to be $6.3 \times 10^4\,M^{-1}$.[21,22]

The spectral changes upon addition of the previously mentioned biologically and environmentally relevant metal

ions were also screened by fluorophotometry and UVVis spectroscopy. The emission and UV/Vis profiles of apo or Pb^{2+}-bound **1** are unchanged in the presence of 10 μM Ca^{2+}, Hg^{2+}, Cd^{2+}, Li^+, Ag^+, Cu^{2+}, Fe^{2+}, Mg^{2+}, Zn^{2+}, K^+, Na^+, Mn^{2+}, Co^{2+}, Fe^{3+}, Al^{3+}, or Ni^{2+} (Figure 2b, S9, and S10), indicating that **1** shows great promise as a useful selective chemosensor for detection of Pb^{2+} in vivo.

We have also investigated the effect of pH on the spectrophotometric behavior of **1** in both the absence and the presence of Pb^{2+} because ideally for biological applications sensing should be practical over a range of pH values. Over the pH range from 3 to 11, **1** showed no fluorescence emission in the absence of Pb^{2+}, whereas upon the addition of Pb^{2+}, **1** displayed strong fluorescence emissions of almost equal fluorescence intensities at all pH values investigated within this range. These results clearly confirm the suitability of **1** for use in physiological environments spanning the range pH 3–11 (Figure S11).

To further demonstrate the practical application of the nanoparticle-based probe **1**, we also established its ability to track Pb^{2+} levels in living cells using a model for respiratory lead exposure. Live-cell confocal microscopy imaging experiments were carried out that utilized **1** to enhance membrane permeability (Figure 3A–C). HeLa cells (human cancer cells) were incubated with **1** (5.0 μM) for 30 min at 37°C, and the cells were then washed with phosphate buffered saline (PBS) to remove excess **1**, which would otherwise contribute to weak intracellular fluorescence (Figure 3B). On treating the HeLa cells with 5.0 μM $Pb(ClO_4)_2$ for 30 min at 37°C and then staining with **1** under the same loading conditions resulted in them exhibiting an increase in observed intracellular fluorescence intensity (Figure 3C). This procedure enabled selective lead ion imaging in living cells to be successfully performed, despite the presence of many potential interfering substances such as proteins and

amino acids. As a consequence, nanoparticles of type **1** are therefore potentially useful for studying the toxicity and/or bioactivity of Pb^{2+} in living cells. We further evaluated the internalization of **1** in HeLa cells by TEM. As shown in Figure S12, intact nanoparticles **1** are primarily seen as confirmed by measurement of their diameters. Conversely, few intact nanoparticles **1** are aggregated. The result provides visual evidence for cellular uptake of fluorescence receptor immobilized $Fe_3O_4@SiO_2$ core/shell nanoparticles **1**.

In addition, we evaluated the reversibility of the above Pb^{2+} detection procedure in living cells. The fluorescence emission of Pb^{2+}-bound **1** was observed to decrease to the initial level value upon addition of EDTA (10 μM) to the HeLa cells. The fluorescence change was reproducible over several cycles of detection/stripping. This result thus strongly indicates that Pb^{2+} ion is dissociated from Pb^{2+}-bound **1** by EDTA. Clearly, chemosensor **1** is not only very useful for detection and removal of toxic Pb^{2+} ion in living cells, but is also able to be readily regenerated using the above procedure. This is the first example of the reversible sensing of a target molecule or ion in living cells.

To quantify the intracellular signalling of **1** within HeLa cells, we examined such cells using analytical flow cytometry (Figure 3D). Flow cytometry revealed that the HeLa cell population treated with **1** in the presence of Pb^{2+} is fluorescent with 10 times more intense fluorescence than the control population in the absence of Pb^{2+} ion. These flow cytometry experiments are in excellent agreement with the confocal imaging results and together confirm the uniform cellular interaction and intracellular signalling of the chemosensor **1**.

In summary, we have readily prepared BODIPY-functionalized $Fe_3O_4@SiO_2$ core/shell nanoparticles **1** by a straight forward procedure. These act as a new type of synthetic fluoro-chromogenic chemosensor for imaging Pb^{2+} ion in living cells. Chemosensor **1** exhibits a high affinity and high selectivity for Pb^{2+} over other competing metal ions tested, and successfully detected Pb^{2+} in cultured cells. These findings show considerable promise for the development of a new category of tailor-made biocompatible sensing systems built by immobilization of appropriate fluoro-chromogenic receptors on the surface of other novel nanomaterials for fluorescence microscopic imaging. They also show considerable promise for the detailed study of the biological action of heavy metal toxins in living systems.
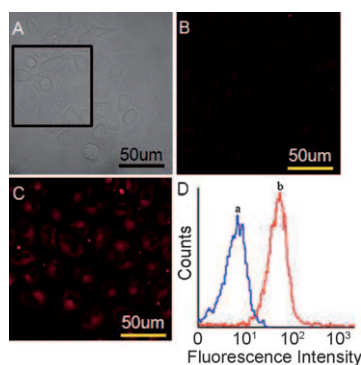

Figure 3. A)–C) Confocal fluorescence images of Pb^{2+} in HeLa cells. The excitation at 635 nm, and the emission is acquired at over 650 nm range. A) Bright-field transmission image of HeLa cells. B) Fluorescence image of HeLa cells incubated with 5 μM **1** for 30 min at 37°C. C) Fluorescence image of **1**-loaded HeLa cells incubated with $Pb(ClO_4)_2$ (5.0 μM) after 30 min at 37°C. D) Fluorescence changes of **1** (5.0 μM) after incubation for 20 min in the a) absence and b) the presence of $Pb(ClO_4)_2$ (5.0 μM) in living cells obtained by flow cytometry analysis; Fluorescence was detected on FL2 channel (excitation: 635 nm, emission: 650 nm). Also, count of 20 000 cells was analyzed.

Experimental Section

suspension and magnetic separation was repeated three times for the purification.

Preparation of 2-immobilized $Fe_3O_4@SiO_2$ (1): Compound **2** (50 mg, 0.054 mmol) was dissolved in anhydrous toluene (5 mL) to which $Fe_3O_4@SiO_2$ core/shell particles (100 mg) was added, and it was stirred under reflux in N_2 for 24 h. The collected solid was washed several times with dichloromethane and acetone to rinse away any excess **2** and then dried under vacuum.

Cell incubation: HeLa cells were cultured in Dulbecco's modified Eagle's medium (DMEM, GibcoBRL, USA) supplied with 10% fetal bovine serum (FBS), 50 μg mL^{-1} penicillin, and 50 μg mL^{-1} streptomycin. The cells were grown on a microscopic culture dish (diameter, 35 mm) with poly-L-lysine coating. To determine the cell permeability of **1**, the cells were incubated with 5.0 μm **1** for 30 min at 37 °C, and washed with phosphate buffered saline (PBS) to remove the remaining **1**. To observe fluorescence changes of the medium, 5.0 μM $Pb(ClO_4)_2$ was added into the **1**-loaded cells and then further incubated for 30 min at 37 °C. The reduction of fluorescence was observed by confocal microscope and flow cytometry analysis.

Fluorescence imaging experiments: Confocal fluorescence imaging was performed with a Zeiss LSM510 Meta laser scanning microscope and a 40× oil-immersion objective lens, using image Pro Plus 5.1 software. Excitation of **1**-loaded cells at 635 nm was carried with HeNe laser, and emission was acquired at over 650 nm range. For all imaging on a microscope, the microscopic incubation chamber (Chamlide TC, LCI, Korea) was used at 37 °C in 5% CO_2 humidified air. In addition, fluorescence intensities were detected on FL2 channel (excitation: 650 nm, e: 564–606 nm) to observe flow cytometry analysis. Count of 20,000 cells was analyzed.

[1] a) R. Krämer, *Angew. Chem.* **1998**, *110*, 804–806; *Angew. Chem. Int. Ed.* **1998**, *37*, 772–773; b) L. Fabbrizzi, A. Poggi, *Chem. Soc. Rev.* **1995**, *24*, 197–202.

[2] H. L. Needleman, *Human Lead Exposure*, CRC Press, Boca Raton, **1992**.

[3] a) S. Araki, H. Sato, K. Yokoyama, K. Murata, *Am. J. Ind. Med.* **2000**, *37*, 193–204; b) N. Rifai, G. Cohen, M. Wolf, L. Cohen, C. Faser, J. Savory, L. DePalma, *Ther. Drug Monit.* **1993**, *15*, 71–74; c) D. A. Cory-Slechta, *Adv. Behav. Pharmacol.* **1984**, *4*, 211–255; d) C. Winder, N. G. Carmichael, P. D. Lewis, *Trends Neurosci.* **1982**, *5*, 207–209.

[4] E. S. Claudio, H. A. Godwin, J. S. Magyar, *Prog. Inorg. Chem.* **2003**, *51*, 1–144, and references therein.

[5] a) Q. He, E. W. Miller, A. P. Wong, C. J. Chang, *J. Am. Chem. Soc.* **2006**, *128*, 9316–9317; b) M. Sun, D. Shangguan, H. Ma, L. Nie, X. Li, S. Xiong, G. Liu, W. Thiemann, *Biopolymers* **2003**, *72*, 413–420; c) J. Liu, Y. Lu, *J. Am. Chem. Soc.* **2003**, *125*, 6642–6643; d) C.-T. Chen, W.-P. Huang, *J. Am. Chem. Soc.* **2002**, *124*, 6246–6247; e) J. Li, Y. Lu, *J. Am. Chem. Soc.* **2000**, *122*, 10466–10467; f) S. Deo, H. A. Godwin, *J. Am. Chem. Soc.* **2000**, *122*, 174–175.

[6] a) Y. H. Zhu, H. Da, X. L. Yang, Y. Hu, *Colloids Surf. A* **2003**, *231*, 123–129; b) D. K. Yi, S. T. Selvan, S. S. Lee, G. C. Papaefthymiou, *J. Am. Chem. Soc.* **2005**, *127*, 4990–4991; c) N. Insin, J. B. Tracy, H. Lee, J. P. Zimmer, R. M. Westervelt, M. G. Bawendi, *ACS Nano* **2008**, *2*, 197–202.

[7] a) A. Abou-Hassan, R. Bazzi, V. Cabuil, *Angew. Chem.* **2009**, *121*, 7180–7183; *Angew. Chem. Int. Ed.* **2009**, *48*, 7316–7319; b) M. Liong, J. Lu, M. Kovochich, T. Zia, S. G. Ruehm, A. E. Nel, F. Tamanoi, J. I. Zink, *ACS Nano* **2008**, *2*, 889–896.

[8] a) A. Descalzo, R. Martínez-Máñez, F. Sancenón, K. Hoffmann, K. Rurack, *Angew. Chem.* **2006**, *118*, 6068–6093; *Angew. Chem. Int. Ed.* **2006**, *45*, 5924–5948; b) W. S. Han, H. Y. Lee, S. H. Jung, S. J. Lee, J. H. Jung, *Chem. Soc. Rev.* **2009**, *38*, 1904–1915.

[9] H. S. Jung, P. S. Kwon, J. W. Lee, J. I. Kim, C. S. Hong, J. W. Kim, S. Yan, J. Y. Lee, J. H. Lee, T. Joo, J. S. Kim, *J. Am. Chem. Soc.* **2009**, *131*, 2008–2012, and references therein.

[10] a) J. Y. Kwon, Y. J. Jang, Y. J. Lee, K. M. Kim, M. S. Seo, W. W. Nam, J. Y. Yoon, *J. Am. Chem. Soc.* **2005**, *127*, 10107–10111; b) P. Chen, B. Greenberg, S. Taghavi, C. Romano, D. Lelie, C. He, *Angew. Chem.* **2005**, *117*, 2775–2779; *Angew. Chem. Int. Ed.* **2005**, *44*, 2715–2719.

[11] a) H. Y. Lee, D. R. Bae, J. C. Park, H. Song, W. S. Han, J. H. Jung, *Angew. Chem.* **2009**, *121*, 1265–1269; *Angew. Chem. Int. Ed.* **2009**, *48*, 1239–1243; b) S. J. Lee, S. S. Lee, J. Y. Lee, J. H. Jung, *Chem. Mater.* **2006**, *18*, 4713–4715; c) S. J. Lee, S. S. Lee, M. S. Lah, J. H. Jung, *Chem. Commun.* **2006**, 4539–4541; d) S. J. Lee, D. R. Bae, W. S. Han, S. S. Lee, J. H. Jung, *Eur. J. Inorg. Chem.* **2008**, 1559–1594.

[12] Y.-Q. Weng, F. Yue, Y.-R. Zhong, B.-H. Ye, *Inorg. Chem.* **2007**, *46*, 7749–7755.

[13] H. J. Kim, S. J. Lee, S. Y. Park, J. H. Jung, J. S. Kim, *Adv. Mater.* **2008**, *20*, 3229–3235.

[14] J. E. Ghadiali, M. M. Stvens, *Adv. Mater.* **2008**, *20*, 4359–4363.

[15] B. J. Melde, B. J. Johnson, P. T. Charles, *Sensors* **2008**, *8*, 5202–5228.

[16] a) E. Climent, M. D. Marcos, R. Martínez-Máñez, F. Sancenón, J. Soto, K. Rurack, P. Amorós, *Angew. Chem.* **2009**, *121*, 8671–8674; *Angew. Chem. Int. Ed.* **2009**, *48*, 8519–8522; b) P. Calelo, E. Aznar, J. M. Lloris, M. D. Marcos, R. Martínez-Máñez, J. V. Ros-Lis, J. Soto, F. Sancenón, *Chem. Commun.* **2008**, 1668–1670; c) J. V. Ros-Lis, R. Casaús, M. Comes, C. Coll, M. D. Marcos, R. Martínez-Máñez, F. Sancenón, J. Soto, P. Amorós, J. E. Haskouri, N. Garro, K. Rurack, *Chem. Eur. J.* **2008**, *14*, 8267–8278.

[17] a) A. Loudet, K. D. Burgess, *Chem. Rev.* **2007**, *107*, 4891–4932; b) A. Coskun, E. U. Akkaya, *J. Am. Chem. Soc.* **2005**, *127*, 10464–10465; c) K. Rurack, M. Kollmannsberger, J. Daub, *Angew. Chem.* **2001**, *113*, 396–399; *Angew. Chem. Int. Ed.* **2001**, *40*, 385–387.

[18] A. P. de Silva, H. Q. N. Gunaratne, T. Gunnlaugsson, A. J. M. Huxley, C. P. McCoy, J. T. Rademacher, T. E. Rice, *Chem. Rev.* **1997**, *97*, 1515–1566.

[19] a) S. C. Dodani, Q. He, C. J. Chang, *J. Am. Chem. Soc.* **2009**, *131*, 18020–18021; b) D. W. Domaille, L. Zeng, C. J. Chang, *J. Am. Chem. Soc.* **2010**, *132*, 1194–1195.

[20] Z. Ekmekci, M. D. Yilmaz, E. U. Akkaya, *Org. Lett.* **2008**, *10*, 461–464.

[21] Association constants were obtained using the computer program ENZFITTER, available from Elsevier-BIOSOFT, 68 Hills Road, Cambridge CB2 1LA (UK).

[22] K. A. Conners, *Binding Constants, The Measurement of Molecular Complex Stability*, Wiley, New York, **1987**.

[23] J. Park, K. An, Y. Hwang, J.-G. Park, H.-J. Noh, J.-Y. Kim, J.-H. Park, N.-M. Hwang, T. Hyeon, *Nat. Mater.* **2004**, *3*, 891–895.